J. Fluid Mech. (2003), *vol.* 494, *pp.* 297–317.
DOI: 10.1017/S0022112003006153 Printed in the United Kingdom

The evaporating meniscus in a channel

By S. J. S. MORRIS

Department of Mechanical Engineering, University of California, Berkeley, CA 94720, USA
morris@me.berkeley.edu

(Received 6 February 2002 and in revised form 3 July 2003)

We consider the evaporating meniscus of a perfectly wetting liquid in a channel whose superheated walls are at common temperature. Heat flows by pure conduction from the walls to the phase interface; there, evaporation induces a small-scale liquid flow concentrated near the contact lines. Liquid is continually fed to the channel, so that the interface is stationary, but distorted by the pressure differences caused by the small-scale flow. To determine the heat flow, we make a systematic analysis of this free-boundary problem in the limit of vanishing capillary number based on the velocity of the induced flow. Because surface tension is then large, the induced flow can distort the phase interface only in a small inner region near the contact lines; the effect is to create an apparent contact angle Θ depending on capillary number. Though, in general, there can be significant heat flow within that small inner region, the presence of an additional small parameter in the problem implies that, in practice, heat flow is significant only within the large outer region where the interface shape is determined by hydrostatics and Θ. We derive a formula for the heat flow, and show that the channel geometry affects the heat flow only through the value of the interface curvature at the contact line. Consequently, the heat flow relation for a channel can be applied to other geometries.

1. Introduction

The problem of the evaporating meniscus in a channel occurs in discussions of micro heat pipes, and steady vapour bubbles in channels (Ha & Peterson 1998; Ajaev & Homsy 2001). In both cases, the evaporation rate is controlled by large temperature gradients near the apparent contact line, and so the thermal field is nearly two-dimensional within each section normal to that line. In steady state, the interface is stationary relative to the wall, so there is no velocity singularity due to a moving contact line. However, there is potentially a thermal singularity. If the solid were isothermal, and the interface temperature equalled the saturation temperature T_o at which the phases coexist at common pressure, the boundary temperature for the liquid would be discontinuous at the contact line. Two mechanisms smooth that discontinuity.

First, because the liquid is chosen to be perfectly wetting in these applications, the part of the solid seeming unwetted to the eye is actually coated by a uniform film, typically a few tens of molecules thick. That wetting film exists because the solid attracts the liquid by van der Waals forces more strongly than it does the vapour. As a result, the phase interface turns parallel to the wall on approaching it. Further, the strong attraction between solid and liquid allows liquid within the film to coexist with its vapour outside, even though the wall temperature T_w exceeds T_o. Wetting physics thus removes the thermal singularity by introducing a minimum film thickness H_s,

and by allowing the interface temperature to vary smoothly from T_w to T_o. Secondly, the interface temperature must exceed T_o to drive evaporation, and must therefore vary with position because the evaporation rate decreases with distance from the contact region. By allowing the interface temperature to vary, evaporation kinetics relax the singularity.

Because the interface in the contact region is distorted by the induced liquid flow, the domain for conduction heat transfer is shaped by a liquid flow whose strength depends on the evaporation rate. The accepted nonlinear theory of the stationary, perfectly wetting, evaporating meniscus therefore couples wetting physics to evaporation kinetics, thin film heat conduction and lubrication theory (Potash & Wayner 1972; Moosman & Homsy 1980). The resulting free-boundary problem contains three parameters. One of these, here denoted by ϵ, is the ratio of the large-scale curvature to the characteristic curvature in the small region where the large-scale interface joins the flat wetting film. Existing analysis (Morris 2001) shows that although the static contact angle vanishes for a perfectly wetting system, an apparent contact angle exists in the limit $\epsilon \to 0$. This angle Θ is a property of the small-scale induced flow; it is determined chiefly by the capillary number based on the characteristic velocity of that flow, and vanishes with capillary number. Because the nonlinear theory is based on the assumption of vanishing interface slope, it holds only if the capillary number is small, as was first pointed out in Morris (2001, p. 18).

To find the heat flow, Stephan & Busse (1992) and Schonberg, Dasgupta & Wayner (1995) informally use the separation of scales allowing the existence of Θ. Those authors divide the meniscus at an arbitrarily chosen point. In a small region near the apparent contact line, the nonlinear theory is used to find Θ, and the local heat flow. Outside that contact region, the induced flow is assumed too weak to distort the interface, whose shape is thus determined by Θ and hydrostatics; the capillary number of the induced flow is thus implicitly taken as small. The outer heat flow is found by solving the conduction equation subject to a simplified interfacial condition on T. That method is informal, as different simplifications are used without explanation. Despite those simplifications, the heat flow across the wall is not found explicitly as a function of superheat; both the inner and outer contributions are computed, and the outer heat flow is a functional of large-scale geometry.

Here, we make a systematic analysis of the free-boundary problem in the limit of vanishing capillary number for a channel whose superheated walls are at common uniform temperature. We derive a formula giving the heat flow q_* per unit width across one wall, and we show that the same formula can be used to find the heat flow per unit length of contact line for any geometry in which the interface curves away from the wall, as in a channel. We then specialize our analysis to the case in which the wetting film thickness H_s (defined precisely by equation (15)), evaporative heat transfer coefficient h (defined by equation (1)), and liquid conductivity K satisfy $\beta = hH_s/K \to 0$; that limit of vanishing micro scale Biot number β is common in applications. By combining existing theory given in Morris (2001) with our new heat flow relation, we prove that for $\beta \to 0$, the dimensionless heat flow $q_*/K(T_w - T_o)$ is uniquely determined by Θ, and the macro scale Biot number defined in terms of the gap thickness $2a$ by $\mathscr{B} = ha/K$.

At this point, we will have used the free-boundary problem to show that, in practice, the heat flow is determined by purely macroscopic variables, rather than by the microphysics included in that model to resolve the thermal contact line singularity. However, because the resulting heat flow relation involves only phenomenological variables, its derivation should be possible without invoking microphysics.

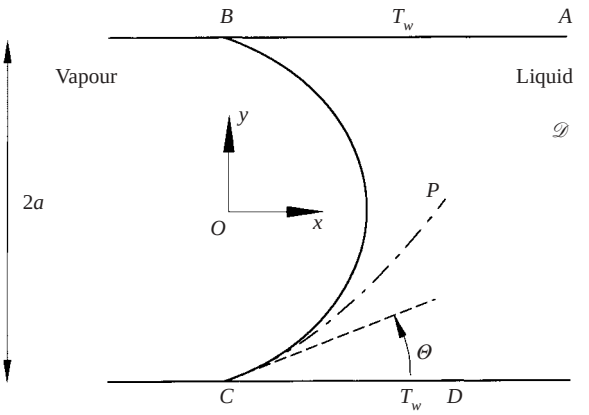

FIGURE 1. Definition sketch.

We use existing theory to obtain such a derivation. In Morris (2000, § 2), self-consistency arguments are used to derive conditions under which there is negligible heat flow at the scale on which the contact angle is established. Those arguments result in a set of three conditions on Θ (treated as a parameter), material properties and the superheat. When these conditions hold, the heat flow can be found by solving the conduction equation for the domain bounded by a circular arc with contact angle Θ; on that arc, Newton's law of cooling holds with a predicted heat transfer coefficient. Because the derivation uses only self-consistency arguments, and is independent of microphysics, this conduction model can be used for finite Θ, even if the system is partially wetting. For the special case of a perfectly wetting system, it is shown in Morris (2001, p. 27) that the self-consistency conditions on Θ are equivalent to the single condition of vanishing micro scale Biot number β. The conduction model and the nonlinear theory thus have a common region of validity, namely for those perfectly wetting systems in which both β and Θ are small.

In § 2, we use the conduction model to find the heat flow for large $\mathscr{B}$, and arbitrary $\Theta \leqslant \pi/2$. (In practice, $\mathscr{B}$ ranges from 40 to about 10^5. The limits $\mathscr{B} \to \infty$ and $\beta \to 0$ are consistent because the wetting film thickness H_s is small compared with the channel thickness $2a$.) We verify our general results for large $\mathscr{B}$ against an exact solution of the conduction model for $\Theta = \pi/2$. In § 3, we analyse the free-boundary problem, and in § 4 we prove that the formulae derived from the two models are asymptotically identical in their common range of validity. In § 5, we give numerical examples showing that the two models agree for parameter values usual in applications, and we show that our predictions agree with the simulation by Schonberg *et al.* (1995). In § 6, we summarize the picture of the evaporating meniscus developed in these papers.

2. Heat flow predicted by the conduction model

Figure 1 shows the evaporating meniscus in a channel of gap thickness $2a$. The phase interface separates the liquid from its pure vapour phase, which is at uniform pressure P_o. The uniform wall temperature $T_w = T_o + \Delta T$, where T_o is the saturation temperature at pressure P_o, and ΔT is the superheat. The (large-scale) phase interface is a circular arc with contact angle Θ. The arc CP is the osculating parabola at C, i.e. the parabolic arc with the same contact angle and curvature as the actual

interface. (At B there is a separate osculating parabola, not shown in the figure.) Liquid of conductivity K fills the region $\mathscr{D}$ to the right of the interface. The latent heat of evaporation is Q. Within the vapour, the sound speed, density and specific heat ratio are, respectively, c, ρ_v and γ; also $\lambda = \sqrt{2\gamma/\pi}$. Material properties are taken as uniform.

In Morris (2000, §2), the kinetic equation and interfacial energy balance are simplified by using scaling to show that, in practice, Newton's law of cooling holds on the interface at scales where there is significant heat flow. That is

$$K\,\partial T_*/\partial n_* + h(T_* - T_o) = 0, \qquad h = \lambda\rho_v Q^2/(c\,T_o) \tag{1a, b}$$

is the evaporative heat transfer coefficient (Cammenga 1980, p. 495), T_* is the dimensional temperature and n_* is normal distance into the vapour. The following must be true for (1) to hold. (i) All heat conducted from the wall to the interface must be absorbed there as latent heat of vaporization. (ii) The evaporation rate at a point on the interface must be independent of the local liquid pressure, so that the Kelvin effect is negligible. (iii) The vapour must be dynamically passive. Examples in Morris (2000, table 1) show that these conditions commonly hold at the scale where there is significant heat flow.

We also assume that pressure variations due to the induced flow are too small to distort the interface at the scale where heat flow occurs. In Morris (2000, p. 64), this is shown to be a good approximation if $Ca \ll \Theta^4$; that condition holds in practice, and for a perfectly wetting system, it is shown in Morris (2001, p. 18) to be valid in the limit $\beta \to 0$. We stress that, at the scale where heat flow occurs, the pressure variations at issue occur within the thin film, not within the half space occupied by vapour.

We define dimensionless variables (without asterisks) by $T = (T_* - T_o)/\Delta T$ and $(x, y) = (x_*, y_*)/a$. The governing equations are

$$\nabla^2 T = 0 \text{ within } \mathscr{D}, \qquad \text{on } |y| = 1, \;\; T = 1; \tag{2a, b}$$

$$\text{on } x^2 + 2x\tan\Theta + y^2 = 1, \qquad (x + \tan\Theta)\frac{\partial T}{\partial x} + y\frac{\partial T}{\partial y} = \mathscr{B}\,T\sec\Theta. \tag{2c, d}$$

Throughout this work, $\nabla^2 = \partial^2/\partial x^2 + \partial^2/\partial y^2$, the macro scale Biot number $\mathscr{B} = ha/K$, and the heat flow per unit width across one wall $q = q_*/K\Delta T$. In (2a), we assume heat flow by pure conduction; this is a good approximation if the Péclet number based on the volumetric evaporation rate and thermal diffusivity is small, as is usually so.

To find q for large $\mathscr{B}$, we let x_1 be a small fixed positive number, and write

$$q = q_{\mathrm{i}} + q_o, \qquad q_{\mathrm{i}} = -\int_0^{x_1} \left.\frac{\partial T}{\partial y}\right|_{y=-1} \mathrm{d}x, \quad q_{\mathrm{o}} = -\int_{x_1}^{\infty} \left.\frac{\partial T}{\partial y}\right|_{y=-1} \mathrm{d}x, \tag{2e}$$

without approximation. We will prove that because x_1 is fixed, for $\mathscr{B} \to \infty$ the outer heat flow q_{o} can be found by setting the interface temperature equal to the constant saturation temperature. However, very near the contact line, T must be allowed to vary along the interface, for otherwise the flux is non-integrable at the contact line. Within that small contact region, other simplifications are possible and allow the inner heat flow q_{i} to be found explicitly. In addition to this inner and outer spatial structure in $T(x, y)$, the function $q(\Theta)$ has itself an inner and outer structure in Θ, as we now show.

2.1. *Outer solution for the function $q(\Theta)$: $\mathscr{B} \to \infty$ with fixed $\Theta \neq 0$*

The outer (spatial) limit is $\mathscr{B} \to \infty$ with (x, y) fixed, and not at the contact lines. In this limit, (2) becomes

$$\nabla^2 T = 0 \text{ within } \mathscr{D}, \quad \text{on } |y| = 1, \ T = 1; \tag{3a, b}$$

$$\text{on } x^2 + 2x\tan\Theta + y^2 = 1, \ T = 0. \tag{3c, d}$$

This problem describes conduction heat flow from the isothermal channel walls to a circular arc on which the dimensional temperature equals the saturation temperature.

In Appendix B, we solve (3) by conformal mapping, and show that with error $o(1)$ in the small quantity x_1, the outer heat flow q_o across the wall between x_1 and ∞ is given by

$$\Theta q_\mathrm{o} = -\ln\frac{x_1}{2\Theta} - 2\ln\left[\sqrt{\pi}\frac{\Gamma(1+\Theta/\pi)}{\Gamma\left(\frac{1}{2}+\Theta/\pi\right)}\right], \tag{4}$$

where $\Gamma(z)$ denotes the usual gamma function. The logarithm occurs in (4) because the boundary temperature is discontinuous at the contact line by (3*b*) and (3*d*), and the film thickness vanishes linearly near the contact line. Together these effects give a flux $\sim x_1^{-1}$, so that the heat flow (integrated flux) varies as $-\ln x_1$.

The flux singularity makes it inconsistent to use the simplified interfacial condition (3*d*) too near the contact line. For the lower contact line in figure 1, the size of that inner region is found by balancing terms in (2*d*) to show that $1 + y \sim 1/\mathscr{B}$ and $x \sim 1/\mathscr{B}$.

We therefore define inner variables by $\hat{x} = \mathscr{B}x, \quad \hat{y} = \mathscr{B}(1+y)$, and define the inner limit as $\mathscr{B} \to \infty$ with $(\hat{x}, \hat{y})$ fixed. In that limit, (2) becomes

$$\frac{\partial^2 T}{\partial \hat{x}^2} + \frac{\partial^2 T}{\partial \hat{y}^2} = 0 \text{ within } \mathscr{D}, \quad \text{on } \hat{y} = 0, \ T = 1; \tag{5a, b}$$

$$\text{on } \hat{y} = \hat{x}\tan\Theta, \quad \sin\Theta\,\frac{\partial T}{\partial \hat{x}} - \cos\Theta\,\frac{\partial T}{\partial \hat{y}} = T. \tag{5c, d}$$

This problem describes conduction heat flow from an isothermal wall across a liquid wedge to a linear interface on which Newton's law of cooling holds. The interface is linear in this small region because the film is now thin compared with the interfacial radius of curvature. In (5), Θ is independent of $\mathscr{B}$, but may be small.

There is no elementary solution of (5) for arbitrary Θ, but in Morris (2000, Appendix A) a regular perturbation expansion in Θ is used to show that the inner heat flow q_i across the wall between $x = 0$ and x_1 is given by

$$\Theta q_\mathrm{i} = \ln(\mathscr{B}\Theta x_1) + \tfrac{1}{18}\Theta^2\left(1 - \tfrac{7}{150}\Theta^2\right) + O(\Theta^6). \tag{6}$$

Figure 4 of Morris (2000) shows that this expression gives the difference $\Theta q_\mathrm{i} - \ln(\mathscr{B}x_1)$ to within 0.7% even for $\Theta = \pi/2$; of course, the error in q_i is much less than that because $\mathscr{B} \to \infty$, so that q_i is determined chiefly by the term in $\ln\mathscr{B}$.

The heat flow across one wall $q = q_\mathrm{i} + q_o$ without approximation. By substituting for q_i and q_o from (4) and (6), we find that for $\mathscr{B} \to \infty$ with fixed non-zero Θ,

$$\Theta q = \ln(2\mathscr{B}\Theta^2) + \tfrac{1}{18}\Theta^2\left(1 - \tfrac{7}{150}\Theta^2\right) - 2\ln\left[\sqrt{\pi}\frac{\Gamma(1+\Theta/\pi)}{\Gamma(\frac{1}{2}+\Theta/\pi)}\right] + o(1). \tag{7}$$

We see that q is independent of the location x_1 at which we divide the interval $0 \leqslant x < \infty$; the dependence on x_1 in the equation for q_o exactly cancels that in the

expression for q_i because the inner and outer problems (3) and (5) are equally valid in the region $\mathscr{B}^{-1} \ll x \ll 1$.

2.2. *Inner solution for the function $q(\Theta)$: $\mathscr{B} \to \infty$ with $\Theta = O(\mathscr{B}^{-1/2})$*

Because the inner interface is taken as linear to derive (7), the result fails when Θ is small enough for the linear and quadratic terms to balance in the Taylor expansion of film thickness about $x = 0$. That failure occurs when $\Theta x \sim x^2$; then $x \sim \Theta$ and the thickness $\sim \Theta^2$. For the left- and right-hand sides of Newton's law ($2d$) to balance, the Biot number based on that thickness must be of order unity, i.e. $\Theta^2\mathscr{B} \sim 1$.

For such small values of Θ, a new analysis of (2) is necessary. We define new inner variables for the lower contact line in figure 1 by $\check{x} = x/\Theta$ and $\check{y} = (1 + y)/\Theta^2$, and define a new inner limit by $\mathscr{B} \to \infty$ (fixed $\Theta^2\mathscr{B}$, $\check{x}$, $\check{y}$). In that limit, (2) becomes

$$\frac{\partial^2 T}{\partial \check{y}^2} = 0 \text{ within } \mathscr{D}, \quad \text{on } \check{y} = 0, \quad T = 1; \tag{8a, b}$$

$$\text{on } \check{y} = \check{x} + \tfrac{1}{2}\check{x}^2, \qquad \frac{\partial T}{\partial \check{y}} + \Theta^2\mathscr{B}\, T = 0. \tag{8c, d}$$

This problem describes conduction heat flow across a quasi-parallel film to a parabolic arc on which Newton's law of cooling applies.

By solving (8), the inner heat flow across the wall between $\check{x} = 0$ and $\check{x} = x_1/\Theta$ is

$$q_i = \frac{2}{\mathscr{A}\Theta} \tanh^{-1} \mathscr{A} - \frac{2}{x_1} + o\,(1)\,, \qquad \mathscr{A}^2 = 1 - 2/(\Theta^2\mathscr{B}). \tag{9a, b}$$

Equation (9) holds for $\mathscr{B} \to \infty$ with $\Theta^2\mathscr{B}$ fixed, but arbitrary; although $\mathscr{A}$ is imaginary for $\Theta^2\mathscr{B} < 2$, q_i remains real by the identity $\tanh^{-1} \mathrm{i}z = \mathrm{i} \tan^{-1} z$. The first term in (9) is large compared with the second, because $\Theta = O(\mathscr{B}^{-1/2})$, but x_1 and $\mathscr{A}$ are fixed.

The outer limit is $\mathscr{B} \to \infty$ with x, y and $\Theta^2\mathscr{B}$ fixed. Newton's law ($2d$) again requires the interface to be isothermal, but now $\Theta = 0$ for the outer problem. From Appendix B, the heat flow across the wall between x_1 and infinity to the semicircular interface

$$q_o = \frac{2}{x_1} - \frac{4}{\pi} \ln 2 + o(1). \tag{10}$$

The x_1-dependence here differs from that in (4), because the outer film thickness now vanishes quadratically rather than linearly with distance from the contact line. The second term in (10) is small compared with the first because x_1 is small.

The heat flow across one wall $q = q_i + q_o$, without approximation. For $\mathscr{B} \to \infty$ with $\Theta^2\mathscr{B}$ fixed, q_i and q_o are given by (9) and (10), so

$$q = \frac{2}{\mathscr{A}\Theta} \tanh^{-1} \mathscr{A} - \frac{4}{\pi} \ln 2 + o(1), \tag{11}$$

and q is again independent of x_1. The first term in (11) is large compared with the second because $\Theta = O(\mathscr{B}^{-1/2})$; the large term represents the heat flow across the parabola osculating with the interface at the contact line, and the smaller second term corrects for the shape of the outer interface. The correction is negative because the actual film is thicker than that below the osculating parabolic, as illustrated in figure 1.

2.3. *Composite expansion giving $q(\Theta)$ for $\Theta \leqslant \pi/2$ and $\mathscr{B} \to \infty$*

Equations (7) and (11) have a common region of validity $\mathscr{B}^{-1} \ll \Theta^2 \ll 1$. In the first case, $\Theta^2\mathscr{B} \gg 1$ so $\mathscr{A} \to 1$, and (11) reduces to

$$\Theta q \sim \ln(2\mathscr{B}\Theta^2) - \frac{4}{\pi}\Theta \ln 2. \tag{12}$$

Because (7) also reduces to (12) for $\Theta^2 \ll 1$, the composite expansion is formed by adding (11) to (7), then subtracting the common part (12).

The heat flow q across one wall is thus given by

$$\Theta q = \frac{2}{\mathscr{A}} \tanh^{-1}\mathscr{A} + \tfrac{1}{18}\Theta^2\left(1 - \tfrac{7}{150}\Theta^2\right) - 2\ln\left[\sqrt{\pi}\frac{\Gamma(1+\Theta/\pi)}{\Gamma\left(\frac{1}{2}+\Theta/\pi\right)}\right] + o(1), \tag{13}$$

where $\mathscr{A}$ is defined by (9). The first term in (13) gives the heat flow for $\Theta \to 0$ across the osculating parabola, i.e. the arc with the same curvature and contact angle at the contact line as the circular arc interface. The second term is the correction to the inner heat flow for finite Θ; and the last term is the correction necessary because the outer interface is not parabolic.

Equation (13) holds for all $\Theta < \pi/2$ and $\mathscr{B} \to \infty$. It is verified by an exact solution of (2) for $\Theta = \pi/2$ (see Appendix A). The exact result has the large-$\mathscr{B}$ asymptote (A 6), namely $\pi q/2 = \ln(4\mathscr{B}/\pi) + \gamma_E + o(1)$, where Euler's constant $\gamma_E = 0.577^+$. For $\Theta = \pi/2$, equation (13) differs only trivially from (A 6), in that the additive constant is given as 0.573 rather than by its true value γ_E.

3. Heat flow predicted by the free-boundary problem

The liquid viscosity and density are μ and ρ_ℓ, and surface tension is σ. The disjoining, or resultant van der Waals, force per unit area acting on an interfacial element is A/Y_*^3 where Y_* is the dimensional film thickness and A is the dispersion constant. As in the conduction model, the pressure in the vapour is taken as uniform. Using the evaporative heat transfer coefficient h, we define a velocity scale V_s for liquid flow normal to the interface and a capillary number Ca by

$$V_s = h\Delta T/(\rho_\ell Q), \qquad Ca = \mu V_s/\sigma. \tag{14a, b}$$

(This scaling differs from that used in the local analysis in Morris (2001): there, all scales are based on the difference $T_w - T_\infty$ between T_w and the temperature T_∞ far from the wall; here, because the channel has finite thickness, we use the superheat $T_w - T_o$.)

Figure 2 outlines the structure which we shall establish for the contact region on the lower wall. The solid curve shows the actual interface shape, and broken curves show the outer limits of the solutions in subregions *Ia* and *Ib*. For vanishing capillary number, $Ca \to 0$, the problem has an inner and outer structure. In the outer region *II* in the figure, the interface is a circular arc because the capillary pressure σ/a is large compared with the characteristic flow pressure $\mu V_s/a$. The thermal boundary condition on that circular arc, and the contact angle, are determined by analysing the contact region *I*.

In region *I*, the interface is perturbed by the induced flow, so that the coupled temperature, pressure and velocity fields are found, together with the interface shape, by solving a free-boundary problem due to Potash & Wayner (1972) and Moosman & Homsy (1980). The dimensional form of that problem is given in Morris (2001, p. 6).

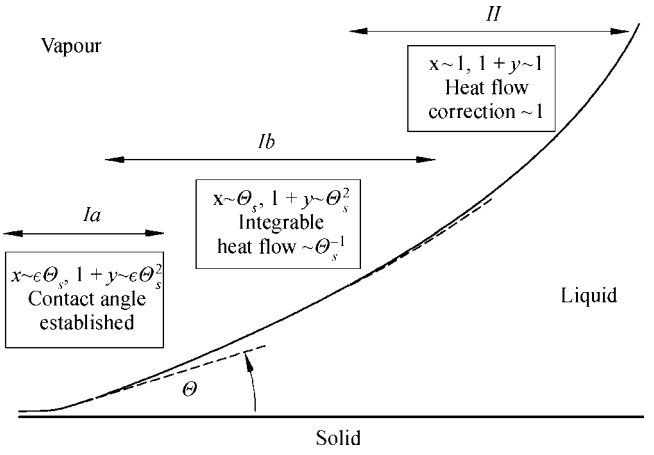

FIGURE 2. Structure of the free-boundary problem for the contact region on the lower wall in the double limit $\Theta_s^2 \to 0$, $\epsilon \to 0$. Coordinates x, y are shown in figure 1. For the slope unit Θ_s, see (15); the apparent contact angle Θ is proportional to Θ_s.

To describe its dimensionless form, given as (20) below, we define the scales

$$P_s = \rho_\ell Q \Delta T / T_o, \quad H_s = (A/P_s)^{1/3}, \quad L_s = (\sigma H_s / P_s)^{1/2}, \quad \Theta_s = H_s / L_s. \tag{15a–d}$$

Below (20), we show that P_s is the pressure difference across the interface of the uniform wetting film shown on the left-hand side of figure 2, and described in § 1; also H_s is the thickness of that uniform film; and L_s is the horizontal scale at which a pressure difference P_s is balanced by surface tension. The contact angle Θ is proportional to the slope unit Θ_s.

We let ΔP be the pressure difference across the interface far from the wall; since $\Theta \ll 1$, ΔP is given in terms of the gap thickness $2a$ by $\Delta P = \sigma / a$. The following parameters appear when the governing equations described above are non-dimensionalized:

$$\epsilon = \Delta P / P_s, \qquad \beta = h H_s / K, \qquad f = 3\mu L_s^2 V_s / \left(P_s H_s^3 \right), \tag{16a–c}$$

as defined in Morris (2001). By (15c), $\epsilon = L_s^2 / (a H_s)$ is the ratio of the curvature a^{-1} of the outer interface to the curvature scale H_s / L_s^2 within the contact region. Also, β is the micro scale Biot number defined in § 1. Lastly, f is the ratio to P_s of the pressure scale $\mu L_s^2 V_s / H_s^3$ of the induced flow.

From the definitions (16), it follows that

$$\Theta_s = (3Ca/f)^{1/4}, \qquad \epsilon \Theta_s^2 = H_s / a, \qquad \epsilon \mathscr{B} \Theta_s^2 = \beta. \tag{17a–c}$$

The important identity (17a) shows that the slope unit vanishes with Ca, so that a small-slope analysis of the contact region is appropriate for $Ca \to 0$ with fixed f and β. We use (17b) below, and we use (17c) in § 4.

To describe the contact region on the lower wall, we define the dimensionless liquid pressure P, film thickness Y and x-coordinate by

$$P = (P_* - P_o)/P_s, \quad Y = (y_* + a)/H_s, \quad X = x_*/L_s. \tag{18a–c}$$

In (18b) and throughout our analysis of the free-boundary problem, y denotes interface location, rather than a coordinate as in § 2; the change is appropriate because here only the interface location is significant, and use of a similar symbol

facilitates comparison with the conduction model. By combining (18) with (17*b*)

$$X = x/(\epsilon\Theta_s), \qquad Y = (1+y)/\left(\epsilon\Theta_s^2\right). \tag{19a, b}$$

This relates the new dimensionless variables to those defined in § 2. For X and $Y \sim 1$, (19) implies that $x \sim \epsilon\Theta_s$ and $1 + y \sim \epsilon\Theta_s^2$, as in figure 2.

3.1. *Boundary-value problem for region I*

We define the inner limit as $\Theta_s^2 \to 0$ with Y fixed. Moosman & Homsy (1980) show that, with error $O(\Theta_s^2)$, in this limit the film thickness Y and liquid pressure P satisfy

$$\frac{\mathrm{d}}{\mathrm{d}X}\left(Y^3\frac{\mathrm{d}P}{\mathrm{d}X}\right) = f\frac{1+P}{1+\beta Y}, \qquad -P = \frac{\mathrm{d}^2Y}{\mathrm{d}X^2} + \frac{1}{Y^3}; \tag{20a, b}$$

$$\text{as } X \to -\infty,\ \frac{\mathrm{d}Y}{\mathrm{d}X} \to 0; \ \text{ as } X \to \infty,\ P \to -\epsilon. \tag{20c, d}$$

The domain is $-\infty < X < \infty$, because there is no contact line for this perfectly wetting system. (This dimensionless version of the problem differs slightly from that in Morris (2001) owing to the present choice of T_o and P_o as reference temperature and pressure.)

We interpret (20). First, the normal stress balance (20*b*) states that in this creeping flow, the pressure force on an interfacial element balances the resultant force due to surface tension and van der Waals forces. Because the interface curves away from the wall, the gas pressure exceeds the pressure in the liquid, making $P < 0$. Secondly, (20*a*) results by combining a mass balance with an interfacial energy balance, one-dimensional heat conduction and evaporation kinetics. This balance states that the liquid flow rate varies along the film owing to the evaporative mass flux expressed by the right-hand side of the equation. The evaporative mass flux varies inversely with Y because the heat flux decreases with increasing film thickness, and also depends on liquid pressure owing to the Kelvin effect, i.e. evaporation is impeded because the gas pressure exceeds that in the liquid. The fluid motion and the heat flow are coupled through the pressure field; the inclusion of this coupling distinguishes the free-boundary problem from the conduction model.

The dimensionless interface temperature is defined by $T_i = (T_{i*} - T_o)/\Delta T$, and is determined as part of the solution of the free-boundary problem. It does not explicitly enter (20), because it has been eliminated algebraically. By equations (6*a*) and (6*b*) of Morris (2001), T_i is given in terms of the film thickness and liquid pressure by

$$T_i = (1 - \beta PY)/(1 + \beta Y). \tag{21}$$

We can now discuss the qualitative nature of the solution of (20). As $X \to -\infty$, the film thickness becomes uniform by (20*c*). Equation (20*b*) then forces P to be constant, and (20*a*) imposes the stronger condition $P \to -1$; so $Y \to 1$. Consequently, P_s is the pressure difference across the equilibrium wetting film, and H_s is the thickness of that film. Next, as X is increased from $-\infty$, Y increases, and P rises above -1, allowing liquid to evaporate. Evaporation ceases as $X \to \infty$, because (20*d*) and (20*b*) together require $Y \sim \epsilon X^2/2$; this parabolic growth makes the right-hand side of (20*a*) vanish as $1/X^2$, and so makes the total evaporation from the contact region I integrable at infinity.

In applications, it is usual that $\epsilon \ll \beta \ll 1$ and $f \sim 1$ (see table 1, and table 1 of Morris 2001). In the limit $\epsilon \to 0$ (with β, f fixed), region I has additional inner and outer structure, which we now derive.

β	f	b	$\ln\delta$
0.029	0.23	1.23	2.98
0.014	1.08	1.90	3.39
0.0064	5.00	2.89	3.81

TABLE 1. Integration constants b and δ obtained by solving the inner problem. Values of β and f are for the conditions of Schonberg *et al.* (1995).

3.1.1. *Region Ia: inner limit* $\epsilon \to 0$ (X, β, f *fixed*)

The inner problem is the special case of (20) with the outer boundary condition (20*d*) replaced by the new boundary condition $P \to 0$ as $X \to \infty$. Then, as shown in Morris (2001, p. 11), equation (20) admits a solution such that as $X \to \infty$,

$$\frac{\mathrm{d}Y}{\mathrm{d}X} = b - \frac{f}{2\beta b^4}\frac{\ln X}{X} + O(X^{-1}), \qquad Y^3\frac{\mathrm{d}P}{\mathrm{d}X} = \frac{f}{\beta b}\ln\left(\frac{X}{\delta}\right) + o(1). \tag{22a, b}$$

The integration constants b and δ are found by solving the inner problem numerically; examples are given in table 1. Because $\mathrm{d}Y/\mathrm{d}X$ approaches a limit at the outer edge of this region, the apparent contact angle is established here; specifically,

$$\Theta = b(3Ca/f)^{1/4}, \tag{22c}$$

where we have used (17*a*). As noted in Morris (2001), the contact angle here is a property of the small-scale flow; unlike the dynamic contact angle of a spreading isothermal drop, it is independent of large-scale geometry.

The linear growth in film thickness predicted by (22*a*) causes the heat flux to decay as $1/X$, and as a result, the total evaporation varies as $\ln X$, as stated by (22*b*). To treat that unbounded growth, Stephan & Busse (1992), and Schonberg *et al.* (1995) use the free-boundary problem to compute only the heat flow across a finite part of the meniscus where the slope is small. They find the rest by numerically solving an outer conduction problem in which the detailed shape of the interface is incorporated, and then patching the two solutions together, in the sense of Van Dyke (1975).

In our matched asymptotic analysis, we incorporate the outer geometry in two steps. We first show that the effect of interface curvature must be included by approximating the interface as a parabolic arc with the same contact angle and curvature as the actual interface at the contact line. Because the interface curves away from the wall, the heat flux decays faster than X^{-1}, and is integrable at infinity. We then calculate the small correction required because the outer circular arc interface is not parabolic for all X.

We now estimate the size of the intermediate region *Ib* in which the interface is approximately parabolic. For any $\epsilon > 0$, the inner solution becomes inconsistent for large X, because (20*d*) and (20*b*) then require $Y \sim \epsilon X^2/2$. For that outer parabolic interface to match smoothly to the outer limit (22) of the inner solution, $bX \sim \epsilon X^2$. Consequently, interface curvature is essential where $\epsilon X \sim 1$, so that $Y \sim \epsilon^{-1}$.

We therefore define intermediate variables by

$$\check{X} = \epsilon X, \qquad \check{Y} = \epsilon Y, \qquad \check{P} = P/\epsilon. \tag{23a–c}$$

It is implicit in these definitions that $\epsilon > 0$, so that the interface curves away from the wall. By (19), $\check{X} = x/\Theta_s$ and $\check{Y} = (1+y)/\Theta_s^2$, so that $\check{X}$ and $\check{Y}$ differ from the variables $\check{x}$ and $\check{y}$ of § 2.2 only because the definitions are now based on the known

slope unit Θ_s rather than on the parameter Θ. Because $\check{X}$ and $\check{Y}$ are of unity in this region, $x \sim \Theta_s$ and $1 + y \sim \Theta_s^2$, as illustrated in figure 2.

3.1.2. *Region Ib: intermediate limit* $\epsilon \to 0$, $(\check{X}, \beta, f$ *fixed*)

By writing (20) in terms of the new variables, without approximation,

$$\frac{\mathrm{d}}{\mathrm{d}\check{X}}\left(\check{Y}^3\frac{\mathrm{d}\check{P}}{\mathrm{d}\check{X}}\right) = \epsilon f\frac{1+\epsilon\check{P}}{\epsilon+\beta\check{Y}}, \qquad -\check{P} = \frac{\mathrm{d}^2\check{Y}}{\mathrm{d}\check{X}^2} + \epsilon^2/\check{Y}^3; \tag{24a, b}$$

$$\text{as } \check{X}\to-\infty,\ \check{Y}\to\epsilon;\ \text{as } \check{X}\to\infty,\ \check{P}\to-1. \tag{24c, d}$$

From the right-hand side of (24*a*), we see that for $\epsilon \to 0$ with β fixed (possibly small), the evaporative mass flux in this region is $O(\epsilon)$.

We seek the solution of (24) in the form of the asymptotic series

$$\check{Y} = \check{Y}_0 + \epsilon\ln\epsilon\ \check{Y}_1 + \epsilon\,\check{Y}_2 + o(\epsilon), \qquad \check{P} = -1 + \epsilon\ln\epsilon\ \check{P}_1 + \epsilon\,\check{P}_2 + o(\epsilon), \tag{25a, b}$$

where the coefficients $\check{Y}_0, \check{P}_1, \cdots$ are independent of ϵ. At leading order in this series, $\check{Y}$ and $\check{P}$ are $O(1)$ by the choice of scales. At the next order, the gauge function is found by matching to the inner solution; for large X, the outer limit (22) of the inner solution requires $P = O(X^{-2}\ln X)$; consequently, $P = O(\epsilon^2\ln\epsilon)$ for $X \sim 1/\epsilon$. The choice of $\epsilon\ln\epsilon$ as gauge function in (25) follows because $\check{P} = P/\epsilon$.

We derive matching conditions on the mass flow $Y^3\mathrm{d}P/\mathrm{d}X$. By (25)

$$Y^3\frac{\mathrm{d}P}{\mathrm{d}X} = \check{Y}_0^3\left\{\frac{\mathrm{d}\check{P}_1}{\mathrm{d}\check{X}}\ln\epsilon + \frac{\mathrm{d}\check{P}_2}{\mathrm{d}\check{X}}\right\} + o(1), \tag{26}$$

but by (22*b*), at the outer edge of region I,

$$\frac{\beta b}{f}Y^3\frac{\mathrm{d}P}{\mathrm{d}X} = -\ln\epsilon + \ln\left(\frac{\check{X}}{\delta}\right) + o(1).$$

The matching conditions obtained from these expressions are

$$\lim_{\check{X}\to0}\frac{\beta b}{f}\check{Y}_0^3\frac{\mathrm{d}\check{P}_1}{\mathrm{d}\check{X}} = -1, \qquad \lim_{\check{X}\to0}\left\{\frac{\beta b}{f}\check{Y}_0^3\frac{\mathrm{d}\check{P}_2}{\mathrm{d}\check{X}} - \ln\check{X}\right\} = -\ln\delta. \tag{27a, b}$$

We obtain differential equations for the coefficients $\check{Y}_0, \check{P}_1, \cdots$ by substituting the trial series (25) into the governing equations (24) to show that

$$\frac{\mathrm{d}^2\check{Y}_0}{\mathrm{d}X^2} = 1, \qquad \frac{\mathrm{d}}{\mathrm{d}\check{X}}\left(\check{Y}_0^3\frac{\mathrm{d}\check{P}_1}{\mathrm{d}\check{X}}\right) = 0, \qquad \frac{\mathrm{d}}{\mathrm{d}\check{X}}\left(\check{Y}_0^3\frac{\mathrm{d}\check{P}_2}{\mathrm{d}\check{X}}\right) = f/(\beta\check{Y}_0). \tag{28a–c}$$

The domain is $0 < \check{X} < \infty$, because $\check{X} \to 0$ in the inner limit $\epsilon \to 0$ with X fixed.

By (28*a*), the curvature is constant at leading order because far from the contact region, the induced flow is weak. The mass flow rate is determined by (28*b*) and (28*c*); it is uniform at leading order, but varies at second order owing to the evaporative mass flux $f/(\beta\check{Y}_0)$.

We find the mass flow at leading order by integrating (28*b*), then applying (27*a*) to show that

$$\frac{\beta b}{f}\check{Y}_0^3\frac{\mathrm{d}\check{P}_1}{\mathrm{d}\check{X}} = -1, \tag{29}$$

for all $\check{X}$. By (26), the corresponding mass flow $Y^3\mathrm{d}P/\mathrm{d}X = -(f/\beta b)\ln\epsilon + O(1)$. This

is exactly what would be obtained by substituting $X \sim \epsilon^{-1}$ in the outer limit (22b) of the inner solution; in effect, because the mass flow is uniform in this region to a first approximation, analysis of the region simply imposes a cutoff scale $X \sim \epsilon^{-1}$ allowing us to estimate the total evaporation from the inner solution (22b).

To evaluate the correction (28c) to the mass flow, we need $\check{Y}_o$. By integrating (28a), then matching to the outer limit (22a) of the inner film thickness, we obtain

$$\check{Y}_0 = b\tilde{X} + \tfrac{1}{2}\check{X}^2. \tag{30}$$

The interface is thus parabolic in region Ib, with contact angle imposed by region Ia. The film thickness vanishes at the apparent contact line $\check{X} = 0$ because, as depicted in figure 2, the inner thickness is small, i.e. $O(\epsilon)$, relative to that in region Ib.

The additional evaporation occurring in region Ib is found by integrating (28c), then applying (27b) to show that

$$\frac{\beta b}{f}\check{Y}_0^3\frac{\mathrm{d}\check{P}_2}{\mathrm{d}\check{X}} = \ln 2b - \ln\delta - \ln\left(1 + \frac{2b}{\check{X}}\right). \tag{31}$$

The term $-\ln\delta$ comes from the matching condition (27b), and so accounts for evaporation in the inner region Ia. Other terms in (31) account for evaporation in region Ib. As $\check{X} \to \infty$, (31) approaches a limit because the film thickness grows faster than $\check{X}$ at infinity. The heat flow across the contact region is integrable at infinity, as claimed above (23).

The heat flow across the film between $-\infty$ and fixed location $x_1 \ll 1$ is given by $\Theta q = \beta b Y^3 \mathrm{d}P/(f\mathrm{d}X)$, as shown in Morris (2001, equation (9)); physically, the heat flow q is related to the liquid flow rate $Y^3\mathrm{d}P/\mathrm{d}X$ because all liquid flowing into the contact region is evaporated, and all heat crossing the wall is absorbed as latent heat of evaporation. By (26), (29) and (31) the heat flow across the contact region I

$$q_I = \frac{1}{\Theta}\ln\left(\frac{2b}{\epsilon\delta}\right) - \frac{2}{x_1} + \cdots. \tag{32}$$

We have used (19a) in the form $\check{X}_1 = x_1/\Theta_s$, and we have also used the fact that $\check{X}_1$ is large because x_1 is fixed, but $\Theta_s \to 0$.

3.2. *Region II: outer semicircular interface*

This region is defined by the outer limit $\Theta^2 \to 0$ with x and y fixed. To solve the outer conduction problem, we need the interface shape, contact angle, and a thermal boundary condition on the interface. The interface is a circular arc because the liquid pressure is uniform far from the contact line in the limit of vanishing capillary number. Next, the contact angle is zero because the slope is independent of Ca on the outer meniscus away from the wall, whereas the slope in the film vanishes with Ca. Lastly, the dimensional interface temperature $T_{i*} = T_o$ because in terms of the variables in (23), the interface temperature $T_i = \epsilon(1 - \beta\check{P}\check{Y})/(\beta\check{Y} + \epsilon)$, which approaches ϵ as $\check{Y} \to \infty$, by (24d). For $\epsilon \to 0$, the dimensionless interface temperature therefore vanishes outside the contact region, so that $T_{i*} = T_o$, as claimed above. It follows that the outer temperature T satisfies the outer problem (3) with $\Theta = 0$; consequently, the outer heat flow across the wall from x_1 to infinity is given by (10).

Θ	$10^3\epsilon$	Equation (33)	Schonberg/equation (33)
0.484	4.10	2.99	0.90
0.511	4.03	3.01	0.83
0.528	3.99	3.00	0.80

TABLE 2. Θq for Schonberg's conditions given in table 1. ϵ is found using radius $\mathscr{R} = a/\cos\Theta$.

3.3. *Total heat flow q across one wall*

By adding (32) to (10), the dimensionless heat flow across one wall is given in the double limit $Ca \to 0$, $\epsilon \to 0$ (with fixed β and f) by

$$q = \frac{1}{\Theta}\ln\left(\frac{2b}{\epsilon\delta}\right) - \frac{4}{\pi}\ln 2 + o(1), \qquad \Theta = (3Ca/f)^{1/4}b, \tag{33a, b}$$

where (22*c*) is repeated as (33*b*). This result holds only if $\epsilon > 0$, so that the interface curves away from the wall. The integration constants $b(\beta, f)$ and $\delta(\beta, f)$ are defined by (22); they are found by solving the inner problem defined in § 3.1.1, and are therefore independent of large-scale geometry.

Equations (33*a*) and (33*b*) are two simultaneous equations giving $q = q_*/K\Delta T$ and Θ in terms of the parameters Ca, β, ϵ and f. Of course, (33*a*) does not imply an inverse relation between Θ and the dimensional heat flow q_*, because Θ is a function of ΔT by (33*b*), and q_* is also normalized against ΔT. We give the correct scaling relation between q_* and Θ in § 4.

The first term in (33) represents the heat flow across the contact region extending from the equilibrium film out to the part of the film that is parabolic on the scale of the channel thickness. The total heat flow in that contact region increases with the horizontal scale L_s and varies inversely with film thickness H_s; consequently, the heat flow varies inversely with Θ_s (for fixed ΔT). In addition, as expressed by the logarithmic term in (33*a*), smaller curvatures on the outer interface result in higher total flows because the heat flow across the contact region is made finite only by the curvature of the interface away from the wall. (If the curvature of the interface is taken as zero far from the wall, we return to a local analysis in which the heat flow grows indefinitely with distance without approaching a limit, as in the inner problem (22*b*).) The second term in (33) is the correction accounting for the non-parabolic shape of the interface in the rest of the channel. That geometrically specific correction is negligibly small in the double limit $\Theta \to 0$, $\epsilon \to 0$.

The heat flow across any evaporating meniscus that curves away from the wall is therefore given approximately by the first term in (33*a*). A numerical example shows this approximation to be accurate in practice. In table 2, we show that for the conditions of Schonberg *et al.* (1995), the full equation (33) predicts that $\Theta q \doteqdot 3.00$. The correction $-(4/\pi)\ln 2$ in (33*b*) represents only about 14% of the total heat flow; that correction is even smaller for the small value of ϵ in the example of Stephan & Busse (1992). We conclude that to a good approximation, the heat flow is determined by the contact region alone, and the correction for the outer meniscus is unnecessary. This method for calculating the heat flow across the meniscus was first given, without proof, in Morris & Moreno (1997).

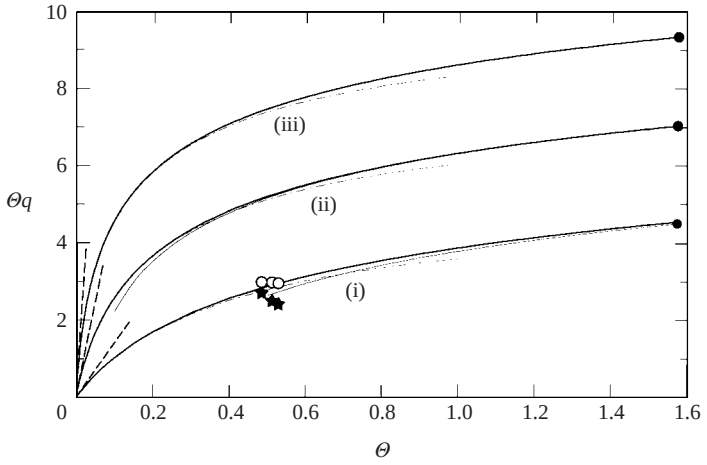

FIGURE 3. Heat flow $q = q_*/(K\Delta T)$ as a function of Θ and $\mathscr{B} = ha/K$. Curves, conduction model for (i) $\mathscr{B} = 40$, (ii) 500, (iii) 5000: heavy curves, composite expansion (13); light curves, fixed-Θ expansion (7); broken curves, small-Θ expansion (11); broken lines, small-Θ limit (35); ●, equation (A 5). Symbols, free-boundary problem: ○, equation (33); ⋆, Schonberg *et al.* (1995).

4. Identity of the models for vanishing micro scale Biot number β

Because the derivation of (33) requires only that $\epsilon \ll \beta$, the result can be used even if β is also small. Further simplification is then possible, because the inner problem for region Ia then has itself an inner and outer structure, whose analysis shows that $\beta b\delta \to 1$ as $\beta \to 0$. (See equation (20) of Morris (2001), and the lines below it; ℓ' there corresponds to δ here.) On substituting for δ in (33), and using (17c) in the form $\epsilon\mathscr{B}\Theta^2 = \beta b^2$, we find that

$$q = \frac{1}{\Theta}\ln(2\mathscr{B}\Theta^2) - \frac{4}{\pi}\ln 2 + o(1), \tag{34}$$

which is identical with the prediction (12) of the conduction model for $\Theta^2\mathscr{B} \to \infty$. (We arrive at the asymptote (12), rather than its parent (11) because in deriving (33), we assumed for simplicity that $\epsilon \ll \beta$; as a result, $\Theta^2\mathscr{B} = \beta b^2/\epsilon$ is large.) We conclude that for vanishing β, the dimensionless heat flow $q = q_*/K\Delta T$ is uniquely determined by the phenomenological variables $\mathscr{B}$ and Θ.

To illustrate (34), we use it to give a scaling argument showing how Θ varies with the dimensional heat flow q_* across the wall. Because, by (21) of Morris (2001), $\Theta \sim (\Delta T)^{1/4}$ to within a factor depending on $\ln\Delta T$, it follows from (34) that $q_* \sim \Theta^3\ln(2\Theta^2\mathscr{B})$, where the second term in (34) has been taken as negligible. Consequently, the contact angle increases with heat flow, as observed experimentally by Kim (1994).

5. Comparison of predicted heat flows for small non-zero β

Figure 3 shows the comparison of the two models analysed here. As defined following (2), the dimensionless heat flow from one wall to the interface $q = q_*/K\Delta T$, and the macro scale Biot number $\mathscr{B} = ha/K$. Heavy curves show the solution (13)

of the conduction model for $\mathscr{B} \to \infty$. The figure includes two tests of the numerical accuracy of that solution. First, for $\Theta = \pi/2$, the large $\mathscr{B}$-solution (13) agrees to within 1% with the exact expression (A 5) given in Appendix A. Secondly, the figure shows the development, with increasing $\mathscr{B}$, of overlap between the small-Θ expansion (11) and the fixed-Θ expansion (7). Even in case (i), for the smallest value of $\mathscr{B} = 40$, the curves for (7) and (11) blend quite smoothly at $\Theta \doteqdot 0.7$, the discrepancy between those curves and that for the composite expansion (13) being only about 6%. In case (iii), for the largest value $\mathscr{B} = 5000$, the curve for (7) is graphically identical with that for (13), and the curves for (7) and (11) overlap for $0 < \Theta < 0.6$. We conclude that (13) predicts the heat flow accurately even for $\mathscr{B}$ as low as 40.

Open symbols in the figure show the prediction (33) of the nonlinear theory for the values of β, ϵ and f given in tables 1 and 2. Those values are for the conditions of Schonberg *et al.* (1995). Because the micro scale Biot number β is small in their examples, the conduction theory and the nonlinear theory should predict the same heat flow. Points computed from (33) agree closely with the prediction of curve (i) from the conduction theory for $\mathscr{B} = 40$. That curve corresponds closely to their examples, for which $h = 4.4$ MW m^{-2} K^{-1}, and $\mathscr{B} = 40.7$. (Values of ϵ in table 2 and this value of $\mathscr{B}$ are based on scales differing by a factor of $\cos\Theta$, and therefore satisfy only approximately the small-Θ relation $\beta b^2 = \epsilon\mathscr{B}\Theta^2$ implied by (17*c*).) Because our new results (13) and (33) give the same heat flow to within a few per cent, we conclude that for these representative values of β, there is indeed negligible heat flow in the innermost region determining Θ.

The figure also shows the results of Schonberg *et al.* (1995). They find q by dividing the meniscus in two, as discussed in § 1. Though their method gives a heat flow whose accuracy is limited only by the resolution of the numerical scheme, they find Θ from the slope at the arbitrarily chosen patching point. Because they patch at very small thicknesses, the contact angle is not fully established and is underestimated; for their conditions, we compute angles about 20% larger than theirs. To plot their heat flows, we use their values of q, but our values for Θ given in table 2. When plotted in this way, their results are in fair agreement with (33).

The behaviour of q near the origin in figure 3 is also interesting. By (13),

$$\lim_{\Theta \to 0} q = \pi\sqrt{\mathscr{B}/2}; \tag{35}$$

for small Θ, the heat flow is algebraically large in the large parameter $\mathscr{B}$ rather than merely logarithmically large, as (34) shows to be the case for fixed $\Theta \neq 0$. Physically, small contact angles correspond to larger heat flows, if all else is equal, because the film remains thin over large horizontal distances. The asymptote (35) is approached in experiments by Kim (1994). In my analysis of those experiments, I show that in one case the macro scale Biot number $\mathscr{B} = 3\,300$, and the measured contact angle $\Theta = 0.014$ (Morris 2001, table 2, row 4). For those values, (13) predicts that $q = 95$, which is within 25% of the limiting value of 128 given by the asymptote (35). It is interesting that this dimensionless heat flow is ~ 25 times that in the example of Schonberg *et al.* (1995) shown in figure 3. Of course, in the experiments, the corresponding dimensional heat flow is only a fraction of a milliwatt, because the small contact angle results from an extremely small superheat of less than a millikelvin. However, the example suggests that very large heat flows might be possible if the wall could be designed to keep Θ small even at larger superheats.

6. Discussion

In this paper, we use two models to predict the heat flow in a channel. Our main new results are (13) and (33), which we derive respectively from the conduction model and the free-boundary problem. We prove that those formulae become identical in the double limit of vanishing micro scale Biot number β and contact angle. From this result, it follows that the heat flow across an evaporating, perfectly wetting meniscus then occurs by pure conduction in a geometry that is established by the apparent contact angle. Because the conduction model can be derived by self-consistency arguments, as shown in Morris (2000), the essential function of the free-boundary model is to provide a relation between Θ and the capillary number of the induced flow. Lastly, we prove that when Θ is small, the heat flow across any meniscus that curves away from the wall, like that in a channel, is determined purely by the contact region. Consequently, we were able to prove that large-scale geometry affects the heat flow only through the interface curvature at the apparent contact line, so that there is a universal relation between the heat flow, Θ, interface curvature, superheat and material properties. This universal relation extends our new results from the channel to other geometries.

For simplicity, we analyse the free-boundary problem only for the case $\epsilon \ll \beta$; for that limit, the universal relation is obtained by deleting the second term from (33). For the conduction model, the corresponding formula for q is

$$\Theta \mathscr{A} q = 2 \tanh^{-1} \mathscr{A}, \qquad \mathscr{A}^2 = 1 - 2/(\Theta^2 \mathscr{B}), \tag{36a, b}$$

by (13) and (9b). Here $\mathscr{B} = h\mathscr{R}/K$, where $\mathscr{R}$ is the interface radius of curvature at the apparent contact line. (A procedure for estimating $\mathscr{R}$ from measured film thickness profiles is given in §§3 and 10 of Morris 2001; there, (36) is used, without proof, to analyse experiments by Kim 1994.) Although (36) could be derived by modelling the evaporating meniscus as a quasi-parallel film bounded by a parabolic interface on which Newton's law of cooling holds, we have derived that simple model from a more generally accepted model, and have provided an estimate of the error made by using (36).

In addition to providing formulae for the heat flow and contact angle, these analyses yield the following robust model of the evaporating meniscus of a perfectly wetting system. Because the microscale Biot number β is small in practice, heat flow occurs at a scale large compared with that on which the contact angle Θ is established. As a result, the heat flow is uniquely specified by macroscopic variables, specifically by Θ and the macro scale Biot number $\mathscr{B}$. Microphysics affects only the relation between Θ and the capillary number Ca of the induced flow. As shown in Morris (2001, §8), for $\beta \to 0$ the contact angle $\Theta = Ca^{1/4}\mathrm{fn}(B)$, where the parameter B depends on a length scale set by microphysics, and vanishes with β. Because $\lim_{B\to 0} \mathrm{fn}(B)$ does not exist, Θ is not uniquely determined by Ca, and microphysics must be included in formulating the free-boundary problem. However, because $\mathrm{fn}(B)$ diverges only weakly as $B \to 0$, the relation between Θ and Ca is insensitive to the precise way in which microphysics is incorporated. That insensitivity results because both Ca and β are small. In the analogous theory of isothermal spreading of a drop, spreading rates are known to be insensitive to the specific microphysical mechanism invoked to relax the velocity singularity at the moving contact line. The papers in this series extend that result to include evaporation.

Insensitivity to microphysical detail is important here, because several premises of the nonlinear theory can fail at the smallest scales of motion if the superheat

is sufficiently large. One example, out of several possible, is that the continuum hypothesis can fail for the vapour because the molecular free path Λ is independent of superheat, whereas the minimum flow scale decreases with increasing superheat. (The continuum hypothesis is not at issue at the larger scales where heat flow occurs; see examples in table 1 of Morris 2000.) The two scales become comparable at superheats occurring in some applications; in the study by Schonberg *et al.* (1995), $\Lambda \sim 10$ nm, and the superheat $\Delta T \sim 5$K corresponds to $L_s \sim 1$ nm. Although the vapour is taken as dynamically passive in the free-boundary problem, the continuum hypothesis is still required because the treatment of evaporation kinetics assumes the existence of a well-defined gas pressure. In fact, the failure of the continuum hypothesis has an additional significance, because by using self-consistency arguments like those in Morris (2000, § 2.3), it can be shown that the vapour is dynamically passive at the smallest scales only if the continuum hypothesis holds there. Because many of the assumptions of the free-boundary model can fail at the smallest scales, it is important that the small-scale motion affects the contact angle only weakly, and has no direct effect on the heat flow. This conclusion also holds for partially wetting systems, as we will show in a paper to follow.

I thank the referees and the associate editor for helpful comments.

Appendix A. Exact solution of (2) for $\Theta = \pi/2$

Liquid now occupies the strip $x > 0$, $|y| < 1$. Let

$$\chi(x, y) = -\partial T/\partial x + \mathscr{B} T. \tag{A 1}$$

By (2), χ satisfies

$$\nabla^2 \chi = 0 \text{ within } \mathscr{D}; \quad \text{on } |y| = 1,\ \chi = \mathscr{B}; \tag{A 2a, b}$$

$$\text{on } x = 0,\ \chi = 0. \tag{A 2c}$$

Problems (2) and (A 2) are equivalent, because it can be shown that if χ satisfies (A 2), and T is finite at infinity, then the function T obtained by integrating (A 1) satisfies (2).

By integrating (A 1), and requiring T to be finite at infinity,

$$T(x, y) = \mathrm{e}^{\mathscr{B}x} \int_x^\infty \mathrm{e}^{-\mathscr{B}\xi} \chi(\xi, y)\, \mathrm{d}\xi. \tag{A 3}$$

Though χ is discontinuous at the vertices of the strip, $T(0, y)$ is continuous because it is obtained by integrating the finite quantity χ along a path of constant y from the uniform state $T = 1$ at infinity.

The flow q across one wall is equal to that across half the interface, so $q = \mathscr{B} \int_0^1 T(0, y)\, \mathrm{d}y$. By using (A 3), interchanging the order of integration, then integrating by parts in ξ,

$$q = \int_0^\infty \mathrm{e}^{-\mathscr{B}\xi} \int_0^1 \frac{\partial \chi}{\partial \xi}(\xi, y)\, \mathrm{d}y\, \mathrm{d}\xi. \tag{A 4}$$

By using the solution of (A 2) given in Carslaw & Jaeger (1959, p. 164) to evaluate the inner integral,

$$q = \frac{2}{\pi} \int_0^\infty \mathrm{e}^{-\zeta} \ln \coth\left(\frac{\pi\zeta}{4\mathscr{B}}\right) \mathrm{d}\zeta. \tag{A 5}$$

This result is used in figure 3.

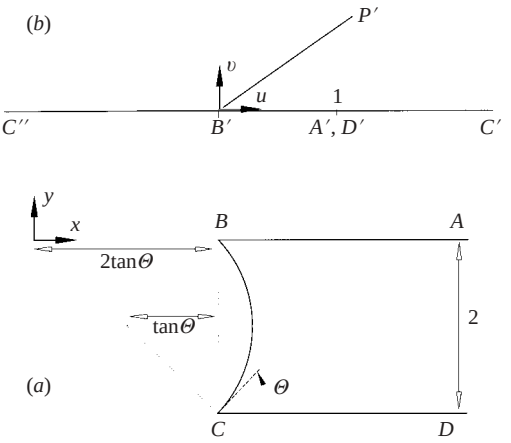

FIGURE 4. The conformal mapping used to solve (3).

For $\mathscr{B} \to \infty$, the argument of the logarithm in (A 5) can be replaced by $4\mathscr{B}/(\pi\zeta)$, giving

$$\tfrac{1}{2}\pi q = \ln\left(\frac{4\mathscr{B}}{\pi}\right) + \gamma_E + o(1)\,; \qquad \gamma_E = -\int_0^\infty \mathrm{e}^{-x} \ln x \,\mathrm{d}x \tag{A 6}$$

is Euler's constant. This result is used below (13). It can be shown numerically that q approaches this asymptote to within 5% for $\mathscr{B} > 2$.

Appendix B. Exact solution of (3) by conformal mapping

Figure 4 shows the geometry of the mapping. With $z = x + \mathrm{i}y$, we show that a function $w(z) = u + \mathrm{i}v$ exists such that curve $ABCD$ in the z-plane maps to the line $\mathrm{Im}\, w = 0$. In the figure, primed and unprimed letters correspond to points and their images. To discuss the map, we take the origin for z on the upper wall, at a distance $2\tan\Theta$ to the left of B.

Let the hypergeometric function

$$F(a, b, c, w) = \frac{\Gamma(c)}{\Gamma(b)\Gamma(c-b)} \int_0^1 t^{b-1}(1-t)^{c-b-1}(1-wt)^{-a}\,\mathrm{d}t, \tag{B 1}$$

as in Abramowitz & Stegun (1970, equation 15.3.1). The parameters a, b and c are dummies occurring only in (B 1). Also $z^p = \exp(p \ln z)$, where the branch cut for $\ln z$ is along the negative real axis, so $-\pi < \arg z \leqslant \pi$. F is singly valued in the w-plane cut along the real axis from 1 to ∞, and is real if a, b, c and w are real with $w < 1$.

Then, the function

$$z = \frac{2\sqrt{\pi}\,\sec\pi\alpha}{\Gamma(1-\alpha)\Gamma\left(\frac{1}{2}+\alpha\right)} \frac{F\left(\frac{1}{2}, \frac{1}{2}-\alpha, 1-\alpha, w\right)}{F\left(\frac{1}{2}, \frac{1}{2}-\alpha, 1, 1-w\right)} \tag{B 2}$$

maps the half plane $\mathrm{Im}\, w > 0$ onto the domain $ABCD$ in figure 4. The contact angle $\Theta = \pi\alpha$.

The claim follows from the properties of the Schwarzian triangle function discussed by Nehari (1975, p. 207). That function maps the half-plane $\mathrm{Im}\, w > 0$ onto a curvilinear triangle whose sides are circular arcs with angles $\alpha\pi$, $\beta\pi$, $\gamma\pi$ at the vertices. To obtain the special case (B 2) of his map, we set $\gamma = 0$ to make the walls

parallel, and then set $\beta = \alpha$. However, (B 2) differs from his map in two respects. To make z our physical coordinate, we have interchanged z and w in his function. We have also multiplied his function by $2\sec\pi\alpha$ to make the gap thickness 2, as in figure 4. Because his result holds for $\alpha + \beta + \gamma < 1$, (B 2) is valid for $\alpha < 1/2$, i.e. for $\Theta < \pi/2$.

Nehari shows that (B 2) maps the half-plane $\operatorname{Im} w > 0$ onto the domain $ABCD$, but does not determine the channel thickness. To prove that the thickness is 2, we show that $C'D'$ maps onto the half-line $\operatorname{Im} z = -2$, $\operatorname{Re} z > 2\tan\Theta$. Our claim then follows because Nehari shows that the interval $A'B'$ maps onto $\operatorname{Im} z = 0$, $\operatorname{Re} z > 2\tan\Theta$.

B.1. *Proof that the channel thickness is 2*

We first show that for real $w > 1$, the function in the numerator of (B 3),

$$F\left(\tfrac{1}{2}, \tfrac{1}{2} - \alpha, 1 - \alpha, w\right) = w^{\alpha - 1/2}\left\{F\left(\tfrac{1}{2}, \tfrac{1}{2} - \alpha, 1 - \alpha, \frac{1}{w}\right) - \mathrm{i}\sqrt{\pi}\frac{\Gamma(1-\alpha)}{\Gamma\left(\tfrac{1}{2} - \alpha\right)}F\left(\tfrac{1}{2}, \tfrac{1}{2} - \alpha, 1, 1 - \frac{1}{w}\right)\right\}. \quad \text{(B 3)}$$

For real $w > 1$, this gives the real and imaginary parts of the left-hand side because the functions on the right-hand side are then real-valued, by the remark above (B 2).

To prove (B 3), we note that the integrand defining the function on the left-hand side is real if $0 < t < 1/w$, but imaginary if $1/w < t < 1$. The contribution of these subintervals to the integral can be expressed in terms of hypergeometric functions by substituting $\tau = wt$ for $0 < t < 1/w$, and $\tau' = (wt - 1)/(w - 1)$ for $1/w < t < 1$. So

$$F\left(\tfrac{1}{2}, \tfrac{1}{2} - \alpha, 1 - \alpha, w\right) = w^{\alpha}\left\{w^{-1/2}F\left(\tfrac{1}{2}, \tfrac{1}{2} - \alpha, 1 - \alpha, 1/w\right) - \mathrm{i}\sqrt{\pi}\frac{\Gamma(1-\alpha)}{\Gamma\left(\tfrac{1}{2} - \alpha\right)}F\left(\tfrac{1}{2} + \alpha, \tfrac{1}{2}, 1, 1 - w\right)\right\}. \quad \text{(B 4)}$$

Equation (B 3) follows on using identity (15.3.5) of Abramowitz & Stegun to express the last term in (B 4) in terms of a hypergeometric function with argument $1 - 1/w$.

To complete the proof that for real $w > 1$, $\operatorname{Im} z = -2$, we write the denominator of (B 2) in terms of a hypergeometric function with argument $1 - 1/w$, i.e. the same as that of the imaginary part of (B 3). By using identity (15.3.3), then identity (15.3.4) of Abramowitz & Stegun, the function in the denominator of (B 2)

$$F\left(\tfrac{1}{2}, \tfrac{1}{2} - \alpha, 1, 1 - w\right) = w^{\alpha - 1/2}F\left(\tfrac{1}{2}, \tfrac{1}{2} - \alpha, 1, 1 - 1/w\right). \quad \text{(B 5)}$$

By (B 3) and (B 5),

$$z = \frac{2\sqrt{\pi}\sec\pi\alpha}{\Gamma(1-\alpha)\Gamma\left(\tfrac{1}{2} + \alpha\right)}\frac{F\left(\tfrac{1}{2}, \tfrac{1}{2} - \alpha, 1 - \alpha, 1/w\right)}{F\left(\tfrac{1}{2}, \tfrac{1}{2} - \alpha, 1, 1 - 1/w\right)} - 2\mathrm{i}. \quad \text{(B 6)}$$

It follows that $\operatorname{Im} z = -2$ for real $w > 1$, because the first term on the right-hand side is then real by the remark above (B 2). The channel thickness is therefore 2, as claimed.

It remains to show that points C' and C correspond, i.e. as $w \to \infty$, $z \to 2(\tan\Theta - \mathrm{i})$. That follows from (B 6) since $F(1/2, 1/2 - \alpha, 1 - \alpha, 0) = 1$, and $F(1/2, 1/2 - \alpha, 1, 1) = \Gamma(\alpha)/(\sqrt{\pi}\Gamma(1/2 + \alpha))$, by equation (15.1.20) of Abramowitz & Stegun. The claim follows on using the reflection formula for $\Gamma(z)$.

B.2. *Behaviour of the map near the contact line*

This behaviour is needed to find the heat flow. It differs according to whether the film thickness vanishes linearly or quadratically with distance near the contact line, i.e. according as $\alpha > 0$, or $\alpha = 0$. In either case, as $w \to 0$ the numerator of (B 2) is proportional to

$$F\left(\tfrac{1}{2}, \tfrac{1}{2} - \alpha, 1 - \alpha, w\right) = 1 + O(w),$$

but the behaviour of the denominator changes.

B.2.1. *Case* $0 < \alpha < 1/2$

In this case, as $w \to 0$, the function in the denominator

$$\sqrt{\pi} F\left(\tfrac{1}{2}, \tfrac{1}{2} - \alpha, 1, 1 - w\right) = \frac{\Gamma(\alpha)}{\Gamma\left(\frac{1}{2} + \alpha\right)} + \frac{\Gamma(-\alpha)}{\Gamma\left(\frac{1}{2} - \alpha\right)} w^{\alpha} + O(w),$$

by identity (15.3.6) of Abramowitz & Stegun.

By combining the asymptotes for F, then using the binomial theorem, and the reflection formula for $\Gamma(z)$, we find that as $w \to 0$ with $0 < \alpha < 1/2$,

$$z - 2\tan \pi\alpha = C(\alpha) w^{\alpha} + O(w), \qquad C(\alpha) = 2\alpha \left[\frac{\Gamma\left(\frac{1}{2} + \alpha\right)}{\Gamma(1 + \alpha)}\right]^2. \tag{B 7}$$

So, as shown in figure 4(*a*), the contact line at $w = 0$ is located at $z = 2\tan \pi\alpha$ in the z-plane. Further, since $(z - 2\tan \pi\alpha)/w^{\alpha} \to C$ as $w \to 0$, the sector subtending angle $\Theta = \pi\alpha$ at the contact line in the z-plane maps into a half plane.

In the rest of this Appendix, we return to the notation in the text, where x is measured from the contact line, as shown in figure 1. By (B 7), on the axis $\operatorname{Im} w = 0$, the corresponding distance from the contact line in the z-plane

$$x = C(\alpha) u^{\alpha} + O(u). \tag{B 8}$$

B.2.2. *Case* $\alpha = 0$

The denominator of (B 2) is now proportional to

$$\pi F\left(\tfrac{1}{2}, \tfrac{1}{2}, 1, 1 - w\right) = \ln(16/w) + O(w \ln w),$$

by Abramowitz & Stegun (1970, equation 15.3.10). So, as $w \to 0$,

$$z = \frac{2\pi}{\ln(16/w)} + O(w \ln w). \tag{B 9}$$

This is the counterpart for $\alpha = 0$ of (B 7). In particular, $w = 0$ corresponds to $z = 0$. Also, by letting $w = r\mathrm{e}^{\mathrm{i}\pi}$ in (B 9) and expanding for $r \to 0$, we find that the negative $\operatorname{Re} w$-axis near the origin corresponds to the parabola $y = -x^2/2$ near B.

On the positive z-axis near the origin, (B 9) requires

$$\ln u \sim -2\pi/x + 4\ln 2. \tag{B 10}$$

As stated above (B 8), x is now measured from the contact line as in figure 1.

B.3. *Heat flow defined by the outer problem* (3)

In the image plane, T satisfies $\partial^2 T/\partial u^2 + \partial^2 T/\partial v^2 = 0$ for $\operatorname{Im} w > 0$. The boundary conditions are that on the positive u-axis, $T = 1$ while on the negative u-axis, $T = 0$. The solution of that boundary-value problem is $T = 1 - \phi/\pi$, where ϕ is the angle

$P'B'C'$ in figure 4(b); i.e.

$$T = \mathrm{Im}\left\{\mathrm{i} - \frac{1}{\pi}\ln w\right\}. \tag{B 11}$$

As stated below (B 1), the branch cut for $\ln w$ is such that $-\pi < \arg w \leqslant \pi$.

We find the heat flow q_o across the interval $x_1 < x < \infty$ on one wall, where x_1 is a small fixed positive number. In Carslaw & Jaeger (p. 449), it is shown that the total heat flow across the isotherm I_1I_2 is $|S_1 - S_2|$ where S is the harmonic conjugate of T, namely the real-valued function such that $S + \mathrm{i}T$ is analytic in z. By (B 11), $S = -(1/\pi)\ln|w|$, so the heat flow across the interval $u_1 < u < 1$ corresponding to $x_1 < x < \infty$ is

$$q_\mathrm{o} = -\frac{1}{\pi}\ln u_1, \qquad u_1 = w(x_1). \tag{B 12}$$

To calculate q_o, only the behaviour of the map near the contact line B is needed.

By combining (B 8), (B 10) and (B 12), we find that with error $o(1)$ for $x_1 \ll 1$,

$$\Theta q_\mathrm{o} = -\ln\frac{x_1}{2\Theta} - 2\ln\left[\sqrt{\pi}\frac{\Gamma(1+\Theta/\pi)}{\Gamma\left(\frac{1}{2}+\Theta/\pi\right)}\right], \quad \text{for } 0 < \Theta < \pi/2; \tag{B 13a}$$

whereas

$$q_\mathrm{o} = \frac{2}{x_1} - \frac{4}{\pi}\ln 2, \quad \text{for } \Theta = 0. \tag{B 13b}$$

Equation (B 13a) is restated as (4), and (B 13b) as (10).

REFERENCES

Abramowitz, M. & Stegun, I. A. 1970 *Handbook of Mathematical Functions*. Dover.

Ajaev, V. S. & Homsy, G. M. 2001 Three-dimensional steady vapour bubbles in rectangular microchannels. *J. Colloid Interface Sci.* **244**, 180–189.

Cammenga, H. K. 1980 Evaporation mechanisms of liquids. In *Current Topics in Materials Science* (ed. E. Kaldis), chap. 4. North Holland.

Carslaw, H. S. & Jaeger, J. C. 1959 *Conduction of Heat in Solids*. Oxford University Press.

Ha, J. M. & Peterson, G. P. 1998 The heat transport capacity of micro heat pipes. *J. Heat Transfer* **120**, 1064–1071.

Kim, I. Y. 1994 An optical study of the heat transfer characteristics of an evaporating thin liquid film. PhD thesis, Rensselaer Polytechnic Institute, Troy, New York.

Moosman, S. & Homsy, G. M. 1980 Evaporating menisci of wetting fluids. *J. Colloid Interface Sci.* **73**, 212–223.

Morris, S. J. S. 2000 A phenomenological model for the contact region of an evaporating meniscus on a superheated slab. *J. Fluid Mech.* **411**, 59–89.

Morris, S. J. S. 2001 Contact angles for evaporating liquids predicted and compared with existing experiments. *J. Fluid Mech.* **432**, 1–30.

Morris, S. J. S. & Moreno, V. 1997 Systematic analysis of an evaporating wetting meniscus on a smooth surface. ASME HTD-Vol. 349, *Proc. Natl Heat Transfer Conf.* **11**, 51–59.

Nehari, Z. 1975 *Conformal Mapping*. Dover.

Potash, M. & Wayner, P. C. 1972 Evaporation from a two-dimensional extended meniscus. *Intl J. Heat Mass Transfer* **15**, 1851–1863.

Schonberg, J. A., Dasgupta, S. & Wayner, P. C. 1995 An augmented Young–Laplace model of an evaporating meniscus in a microchannel with high heat flux. *Expl Therm. Fluid Sci.* **10**, 163–170.

Stephan, P. C. & Busse, C. A. 1992 Analysis of the heat transfer coefficient of grooved heat pipe evaporator walls. *Intl J. Heat Mass Transfer*, **35**, 383–391.

Van Dyke, M. 1975 *Perturbation Methods in Fluid Mechanics*. Parabolic.